SERIALLY CONCATENATED ARTM TIER I WAVEFORMS WITH ITERATIVE DETECTION

Erik Perrins
Department of Electrical and Computer Engineering
Brigham Young University
Provo, UT 84602
esp@ieee.org

Faculty Advisor:
Michael Rice

ABSTRACT

We investigate the performance of Feher-patented quadrature phase-shift keying (FQPSK) and shaped-offset QPSK (SOQPSK) when serially concatenated with an outer code. We show that the receiver complexity for FQPSK and SOQPSK can be greatly reduced by viewing them as continuous phase modulation (CPM) waveforms. We use the pulse amplitude modulation (PAM) representation of CPM, which allows near-optimum detection of both modulations using a simple 4-state trellis. We compare the performance of the PAM-based approximation with another common approximation known as frequency/phase pulse truncation (PT). We use both of these reduced-complexity designs in serially concatenated coding schemes with iterative detection. In the end, we show that the PAM approximation has a slight performance advantage over PT, but both approximations achieve large coding gains in the proposed serially concatenated systems.

INTRODUCTION

In Offset QPSK (OQPSK), the quadrature component of the modulated carrier is delayed half a symbol time relative to the inphase component to avoid instantaneous 180° phase shifts. This is done to reduce the amount of spectral regrowth when a non-linear power amplifier is used. The spectral containment can be greatly improved by using cross correlated bandwidth efficient pulses, as is the case with Feher-patented QPSK (FQPSK) [2]. Shaped offset QPSK (SOQPSK) is very similar to FQPSK, except that the signal is typically viewed as a continuous phase modulation (CPM) rather than as a cross correlated linear modulation. Versions of these two waveforms, SOQPSK and FQPSK, have been incorporated into

IRIG-106 as the "ARTM Tier I" waveforms [3].

When it comes to detecting the ARTM Tier I waveforms, the usual approach is to use an OQPSK-type detector. This simple (and suboptimal) detector is nothing more than a detection filter followed by a decision device. The primary drawback of this approach is that it ignores the inherent memory of these modulations.

In this paper, we address this problem by using a strict CPM point of view when designing the detector. This is a very straightforward and natural approach for SOQPSK. On the other hand, FQPSK cannot be exactly represented as a CPM; therefore, a very close CPM approximation of FQPSK is used in place of the exact FQPSK model. The primary advantage of this CPM-based approach is that the memory of the signal is properly modeled in the detector. This leads to optimal or near-optimal detectors. Another advantage of the CPM-based approach is that *the modulation itself* can be viewed as a code. Therefore, the CPM-based detector is especially useful when codes are concatenated with the modulation and when iterative (turbo) detection is used.

In the next section we describe the signal model used in the transmitters and receivers. In the section after that we show how the CPM model is used to construct simple, near-optimal detectors for SOQPSK and FQPSK. As we shall see, the CPM model alone is not sufficient to yield low-complexity detectors. Therefore, two well-known complexity-reduction techniques for partial-response CPM are used. The first is the pulse amplitude modulation (PAM) approximation [4], which was recently extended in [5] to ternary CPMs such as SOQPSK. The PAM technique allows the use of the simple 4-state trellis in [1] with a loss of only 0.1 dB in the uncoded case. The second reduced-complexity option is frequency/phase pulse truncation (PT) [6], which also allows the use of the simple 4-state trellis with a slightly larger loss of 0.2 dB in the uncoded case. The final objective for these reduced-complexity designs is in constructing simple decoders for serially concatenated coded FQPSK and SOQPSK. We show that the proposed CPM-based designs achieve large coding gains which are similar to those reported in [1] for serially concatenated coded military standard (MIL-STD) SOQPSK systems.

SIGNAL MODEL

A. XTCQM (Transmitter) Model

Simon has shown that SOQPSK and FQPSK can each be modeled as slightly different examples of cross-correlated trellis-coded quadrature modulation (XTCQM) [7, 8, 9]. From this point on, when we speak of FQPSK we mean the version presented in [10] (FQPSK-JR). As for SOQPSK, we concentrate on the version in IRIG-106 [3] which is used by the telemetry group (SOQPSK-TG). The signal model for XTCQM is shown in the upper branch of Figure 1. The transmitted bits $a_i \in 0, 1$ have a duration of T_b and are differentially encoded by the function

$$d_i = a_i \oplus d_{i-2} \tag{1}$$

where $\oplus$ is the XOR operator for binary data in the set $\{0, 1\}$. The differentially encoded bits are then

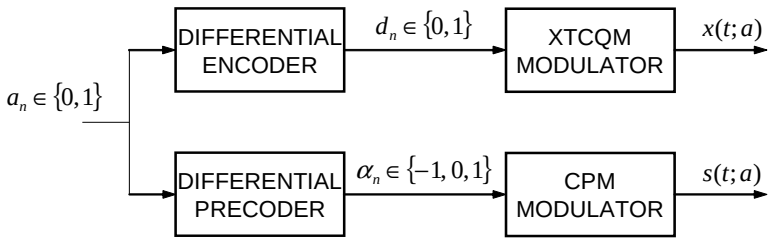

Figure 1: Signal model for uncoded FQPSK-JR and SOQPSK-TG.

transmitted[1] with an offset QPSK-type modulation of the form

$$x(t;\boldsymbol{a}) = \sum_k s_{I,m}(t - kT_s) + j s_{Q,m}(t - kT_s - T_s/2) \tag{2}$$

where $T_s = 2T_b$ and the data-dependent pulses $s_{I,m}(t)$ and $s_{Q,m}(t)$ are each drawn in a constrained way from a finite set of waveforms [8]. For FQPSK-JR, only 16 waveforms are needed to form the signal $x_{\text{JR}}(t;\boldsymbol{a})$ [10]. For SOQPSK-TG, it can be shown that 2048 waveforms are required for $x_{\text{TG}}(t;\boldsymbol{a})$ [12]. For reasons that will be made clear in the next subsection, the XTCQM signal is used to model the transmitter. However, since the focus of this paper is on reducing complexity at the *receiving* end, we do not elaborate further on the XTCQM model and instead refer the interested reader to [8]. Suffice it to say that the *transmitter* sends the signal $x(t;\boldsymbol{a})$, but the *receiver* itself is based on the CPM model for SOQPSK and its approximations.

B. CPM (Receiver) Model

The signal model for SOQPSK is shown in the lower branch of Figure 1. The bits $a_i \in 0, 1$ are first differentially encoded by (1), which is then followed by a *precoder* which operates on the original bits and the differentially encoded bits like so

$$\alpha_i = (-1)^i a_i d'_{i-1} d'_{i-2} \tag{3}$$

where $d'_i \in \{-1, 1\}$ is the antipodal counterpart of d_i and is given by $d'_i = 2d_i - 1$. We refer to the concatenation of (1) and (3) as the *differential precoder*, as shown in Figure 1. Although given in equation form in (3), this differential precoder is the same as the one shown as a block diagram in [1, Fig. 7]. The output of the precoder is α_i, which takes on values in the ternary alphabet $\{-1, 0, 1\}$ and is constrained in the following way: 1) While α_i is viewed as being *ternary*, in any given bit interval α_i is actually drawn from one of two *binary* alphabets, $\{0, 1\}$ or $\{0, -1\}$, 2) When $\alpha_i = 0$, the binary alphabet for α_{i+1} switches from the one used for α_i, when $\alpha_i \neq 0$ the binary alphabet for α_{i+1} does not change, and 3) A value of $\alpha_i = 1$ can not be followed by $\alpha_{i+1} = -1$, and vice versa (this is implied by the previous constraint).

With α_i defined as a function of a_i, the SOQPSK signal is represented as a CPM [13]

$$s(t;\boldsymbol{a}) = \exp\{j\phi(t;\boldsymbol{a})\} \tag{4}$$

[1]The differential encoder is not a necessary component of the XTCQM model. It is used in this paper so that large interleaver gains are obtained in the proposed serially concatenated systems [11].

where the phase is a pulse train of the form

$$\phi(t;\boldsymbol{a}) = 2\pi h \sum_i \alpha_i q(t - iT_b)$$

and the modulation index is $h = 1/2$. The *phase pulse* $q(t)$ is usually thought of as the time-integral of a *frequency pulse* $f(t)$ with area 1/2 and duration LT_b. When $L = 1$ the signal is *full-response* and when $L > 1$ it is *partial-response*. Due to the constraints on $f(t)$ and $q(t)$, the phase may be expressed as

$$\phi(t;\boldsymbol{a}) = \underbrace{2\pi h \sum_{i=n-L+1}^{n} \alpha_i q(t - iT_b)}_{\theta(t)} + \underbrace{\pi h \sum_{i=0}^{n-L} \alpha_i}_{\theta_{n-L}} \tag{5}$$

where $nT_b \le t < (n+1)T_b$. The *phase state* θ_{n-L} can only assume $p = 4$ distinct values[2] given by the look-up table

$$\theta[\eta] = \frac{2\pi\eta}{p}, \qquad 0 \le \eta \le p-1.$$

In (5), we have $\theta_{n-L} = \theta[I_{n-L}]$, where the *phase state index* is

$$I_{n-L} = \left(\sum_{i=0}^{n-L} \alpha_i \right) \bmod p. \tag{6}$$

The SOQPSK versions differ by their respective frequency pulses. With SOQPSK-TG, the frequency pulse has a duration of $L_{\text{TG}} = 8$ bit times and is given by

$$f_{\text{TG}}(t) = A \frac{\cos\left(\frac{\pi\rho Bt}{2T_b}\right)}{1 - 4\left(\frac{\rho Bt}{2T_b}\right)^2} \times \frac{\sin\left(\frac{\pi Bt}{2T_b}\right)}{\frac{\pi Bt}{2T_b}} \times w(t) \tag{7}$$

where the window is

$$w(t) = \begin{cases} 1, & 0 \le \left|\frac{t}{2T_b}\right| < T_1 \\ \frac{1}{2} + \frac{1}{2}\cos\left(\frac{\pi}{T_2}\left(\frac{t}{2T_b} - T_1\right)\right), & T_1 \le \left|\frac{t}{2T_b}\right| \le T_1 + T_2 \\ 0, & T_1 + T_2 < \left|\frac{t}{2T_b}\right|. \end{cases}$$

The constant A is chosen to give the pulse an area of 1/2 and $T_1 = 1.5$, $T_2 = 0.5$, $\rho = 0.7$, and $B = 1.25$. Figure 2(a) shows the frequency pulse in (7) and the corresponding phase pulse $q_{\text{TG}}(t)$. For SOQPSK-TG, it can be shown that $x_{\text{TG}}(t;\boldsymbol{a}) = s_{\text{TG}}(t;\boldsymbol{a})$. Therefore, either output in Figure 1 can be used to transmit SOQPSK-TG.

[2]We use $\alpha_i \in \{-1, 0, 1\}$ and $h = 1/2$ to be consistent with previous work with SOQPSK. This notation is in conflict with traditional CPM notation, which calls for $\alpha_i \in \{-2, 0, 2\}$ when the data alphabet is ternary [14]. Thus, in strict CPM terms, we really have $h = 1/4$, which is why there are $p = 4$ phase states.

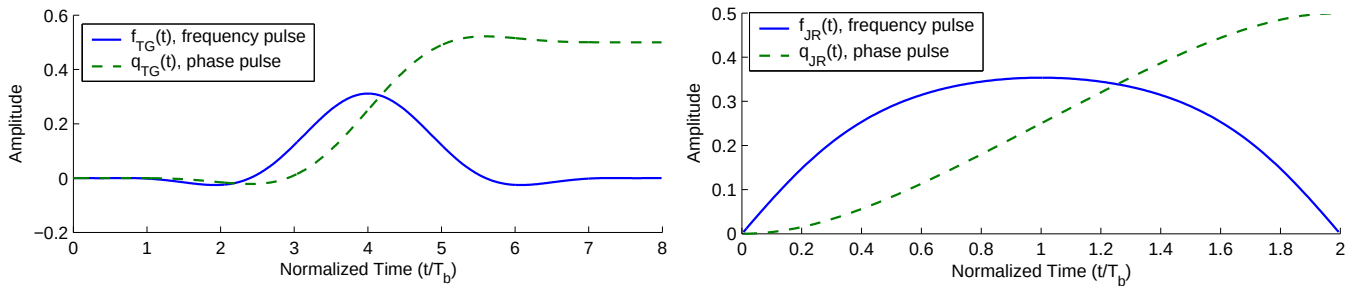

(a) (b)

Figure 2: Frequency and phase pulses for (a) SOQPSK-TG and (b) the CPM approximation of FPQSK-JR.

This is not the case for FQPSK, which cannot be exactly represented with a CPM model. However, a very close CPM approximation can be obtained with $x_{\text{JR}}(t;\boldsymbol{a}) \approx s_{\text{JR}}(t;\boldsymbol{a})$, where $s_{\text{JR}}(t;\boldsymbol{a})$ has the frequency pulse [12]

$$f_{\text{JR}}(t) = \frac{\frac{A\pi}{2T_b}\sin\left(\frac{\pi t}{2T_b}\right)}{\sqrt{1 - A^2\cos^2\left(\frac{\pi t}{2T_b}\right)}} \tag{8}$$

which has a duration of $L_{\text{JR}} = 2$ bit times. Figure 2(b) shows the frequency pulse in (8) and the corresponding phase pulse $q_{\text{JR}}(t)$.

Since the CPM model does not support an exact representation of both modulations (FQPSK and SOQPSK), we ignore the lower branch in Figure 1 for the purposes of conceptualizing the transmitter. Therefore, the signal that arrives at the receiver is modeled as

$$r(t) = x(t;\boldsymbol{a}) + n(t)$$

where $n(t)$ is complex-valued additive white Gaussian noise with single-sided power spectral density N_0. This is the received signal model that will be used in the remainder of the paper. On the other hand, for the purposes of conceptualizing the detectors, we are free to use $s(t;\boldsymbol{a})$ and its approximations, which proves to yield simple near-optimum detectors.

DETECTION ARCHITECTURES

A. 4-State Trellis

We now turn our attention to the trellis needed to describe the differential precoder and the CPM modulator in Figure 1. Using d_{n-1}, d_{n-2}, and n-even/n-odd from (3) as state variables, it is clear that the differential precoder can be described with an 8-state trellis. If we construct a *time-varying* trellis, with different sections for n-even and n-odd, then we have the 4-state trellis shown in Figure 3. The state variables are d_{n-1} and d_{n-2}. They are ordered (d_{n-2}, d_{n-1}) for n-even and (d_{n-1}, d_{n-2}) for n-odd, so that the inphase bit is always most-significant.

It can be shown that the 4-state trellis in Figure 3 not only describes the differential precoder, but also the concatenation of a *full-response* CPM modulator. This is because the only state variable required

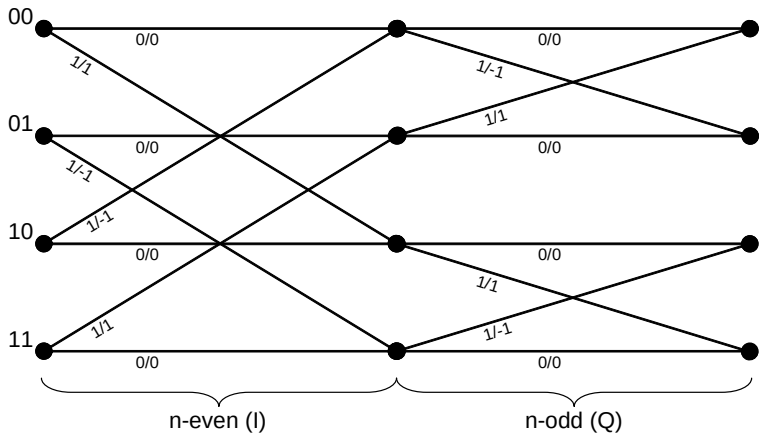

Figure 3: 4-state time-varying trellis for the differential precoder. The labels along the l-th branch at time index n are for the input bit/output symbol pair $a_{l,n}/\alpha_{l,n}$.

by a full-response CPM scheme is the phase state index I_{n-1} in (6), which is simply another way of expressing the two most recent outputs, d_{n-1} and d_{n-2}, of the differential encoder in (1). In other words, the differential precoder and the full-response CPM modulator require the same state variables. This is shown graphically in Figure 4, which shows the one-to-one mapping between the state values, in the set $\{00, 01, 10, 11\}$, and the CPM phase state indexes, in the set $\{0, 1, 2, 3\}$. It is evident that the CPM phase states are a $\pi/4$-rotated version of the traditional QPSK constellation. The result of this observation is that the 4-state trellis in Figure 3 is the natural and optimal trellis for full-response SOQPSK, such as MIL-STD SOQPSK [15, 1]. With partial-response SOQPSK, each additional increment of L results in an additional binary-valued state variable [13, Ch. 7]; in other words, the number of states grows exponentially as L increases. For SOQPSK-TG, this amounts to 512 states. Due to this unmanageable number of states, we are interested in complexity-reduction techniques that allow us to use the simple 4-state full-response trellis in Figure 3 on the receiving end, even though the transmitter is sending a partial-response signal. We explore two such methods now.

B. PAM-based Detector for SOQPSK

We construct a PAM-based detector as follows. We index the 8 branches of the trellis in Figure 3 with $l \in \{0, \ldots, 7\}$. For a given l there is a starting state $S_l \in \{00, 01, 10, 11\}$ and a corresponding phase state index $P_l \in \{0, 1, 2, 3\}$, where the mapping between the two is shown in Figure 4. The l-th branch also has an ending state $E_l \in \{00, 01, 10, 11\}$.

For a given l and n there is a branch bit $a_{l,n}$ and a branch symbol $\alpha_{l,n}$. With these branch quantities defined, the branch metric increment for the PAM-based detector is

$$z_{\text{PAM}}(l, n) = \text{Re}\left[e^{-j\theta[P_l]} \sum_{k=0}^{1} y_k(n)(\beta_{k,n}^l)^*\right]. \tag{9}$$

The values $\beta_{k,n}^l$ are called the branch *pseudo-symbols*. For a given value of the ternary branch symbol $\alpha_{l,n}$ there are two branch pseudo-symbols, $\beta_{0,n}^l$ and $\beta_{1,n}^l$, as shown in Table 1 [5]. The operation $(\cdot)^*$ is the

State	P_l
00	3
01	2
10	0
11	1

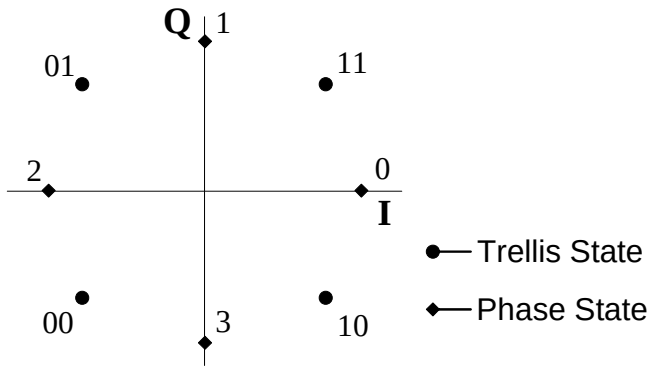

Figure 4: The mapping between the trellis states and the phase state index.

Table 1: The relationship between the ternary branch symbol $\alpha_{l,n}$, the bits $\gamma_{1,l}$ and $\gamma_{0,l}$, and the pseudo-symbols $\beta^l_{k,n}$ for SOQPSK.

$\alpha_{l,n}$	$\gamma_{1,l}$ $\gamma_{0,l}$	$\beta^l_{0,n}$	$\beta^l_{1,n}$
-1	-1 -1	$\exp\{-j\pi/2\} = -j$	$\exp\{-j\pi/4\} = \frac{\sqrt{2}}{2}(1-j)$
0	-1 1, or 1 -1	1	$\cos(\pi/4) = \frac{\sqrt{2}}{2}$
1	1 1	$\exp\{j\pi/2\} = j$	$\exp\{j\pi/4\} = \frac{\sqrt{2}}{2}(1+j)$

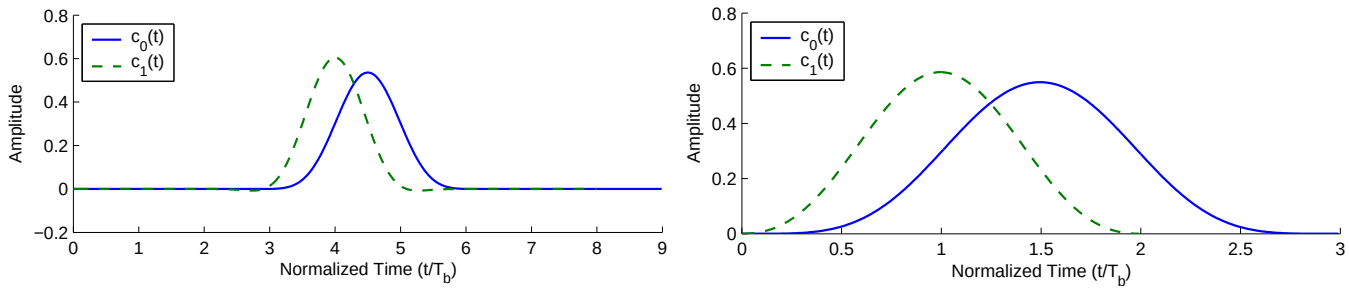

(a) (b)

Figure 5: The two principal pulses for the PAM approximation of (a) SOQPSK-TG and (b) FQPSK-JR.

complex conjugate. The sampled matched filter output is

$$y_k(n) = \int_{nT_b}^{(n+D_k)T_b} r(t)c_k(t - nT_b)\, dt \tag{10}$$

where the two matched filters (pulses) are given by [5]

$$\begin{aligned} c_0(t) &= \left(\prod_{v=0}^{L-1} u(t+vT_b)\right)^2 \\ c_1(t) &= 2\left(\prod_{v=0}^{L-1} u(t+vT_b)\right)\left(\prod_{v=0}^{L-1} u(t+vT_b+T_b)\right) \end{aligned} \tag{11}$$

with

$$u(t) = \begin{cases} \sin\left(2\pi hq(t)\right) / \sin(\pi h), & 0 \le t < LT_b \\ \sin\left(\pi h - 2\pi hq(t-LT_b)\right) / \sin(\pi h), & LT_b \le t < 2LT_b \\ 0, & \text{otherwise.} \end{cases}$$

These pulses are shown in Figure 5 for SOQPSK-TG and for the CPM approximation of FQPSK-JR in (8). The pulses have a duration of D_k bit times, where

$$D_k = L + 1 - k, \qquad 0 \le k \le 1. \tag{12}$$

The matched filters are implemented with a delay of LT_b since the longest pulse, $c_0(t)$, has a duration of $D_0 = (L+1)T_b$.

The branch metric in (9) is valid for SOQPSK-TG and FQPSK-JR, the only difference between the two is the respective set of pulses in Figure 5. It can be used as the generic branch metric increment $z(l, n)$ in the Viterbi algorithm (VA) [13, Ch. 7], as in

$$\lambda_{n+1}(E_l) = \lambda_n(S_l) + z(l, n) \tag{13}$$

where $\lambda_n(\cdot)$ is the cumulative metric for a given state at index n. We can also use (9) in the soft-input soft-output (SISO) module developed in [16]. In this context we view the SOQPSK signal along the l-th

branch as the codeword c_l. The soft input probability of c_l at index n is [17]

$$P_n[c_l; \text{Input}] \sim \exp\left\{\frac{z(l,n)}{N_0}\right\}. \tag{14}$$

C. Pulse Truncation for SOQPSK

A second method of forcing a full-response trellis for SOQPSK is to use the phase/frequency pulse truncation (PT) technique in [6]. Here the detector is based on the truncated phase pulse

$$q_{\text{PT}}(t) = \begin{cases} 0, & t < 0 \\ q(t + (L-1)T_b/2), & 0 \le t \le T_b \\ 1/2, & t > T_b. \end{cases} \tag{15}$$

The truncation in (15) shortens the phase pulse by a total of $(L-1)T_b$ and is centered such that half of the truncation is applied to the beginning of the pulse and half to the end. Since $q_{\text{PT}}(t)$ only has variations in the time interval $[0, T_b]$, it behaves like a full-response pulse. We can now use the 4-state trellis in Figure 3. The trellis is organized in the same manner as before, with the l-th branch at index n having the phase state index P_l and branch symbol $\alpha_{l,n}$. The branch metric increment for PT is

$$z_{\text{PT}}(l,n) = \text{Re}\left[e^{-j\theta[P_l]} \int_{[n+(L-1)/2]T_b}^{[n+(L+1)/2]T_b} r(t) e^{-j2\pi h \alpha_{l,n} q_{\text{PT}}(t-nT_b)} dt\right] \tag{16}$$

where the matched filters are implemented with a delay of $T_b(L-1)/2$ so that the received signal is centered properly with respect to the truncated phase pulse. As with the PAM-based branch metric increment, (16) can be used in the VA (13) or the SISO module (14).

PERFORMANCE

A. Uncoded Systems

For the uncoded case, the probability of bit error for both FQPSK-JR and SOQPSK-TG is bounded by

$$P_b \le Q\left(\sqrt{d_{\min}^2 \frac{E_b}{N_0}}\right) + Q\left(\sqrt{d_1^2 \frac{E_b}{N_0}}\right) \tag{17}$$

where E_b/N_0 is the bit-energy-to-noise ratio and

$$Q(x) = \frac{1}{\sqrt{2\pi}} \int_x^\infty e^{-u^2/2}\, du. \tag{18}$$

For FQPSK-JR we have $d_{\min}^2 = 1.56$ and $d_1^2 = 2.56$ [18]. For SOQPSK-TG we have $d_{\min}^2 = 1.60$ and $d_1^2 = 2.59$ [19]. Therefore, SOQPSK-TG has a $10\log_{10}(1.59/1.56) = 0.08$ dB performance advantage

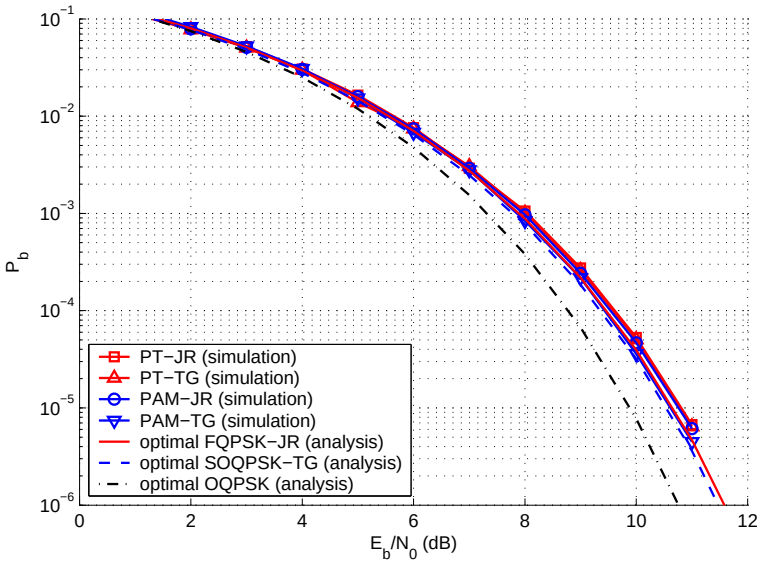

Figure 6: Performance of uncoded systems.

asymptotically over FQPSK-JR. Figure 6 shows the optimal detection curves[3] generated by (17) for both FQPSK-JR and SOQPSK-TG. A reference curve for standard OQPSK ($d^2_{\min} = 2$) is also shown.

We compare these optimal detection curves with simulation results for uncoded FQPSK-JR and SOQPSK-TG, also shown in Figure 6. The fact that the curves are tightly clustered in Figure 6 is evidence that PAM- and PT-based detectors have near-optimum performance. Using $P_b = 10^{-5}$ as a reference point, the losses for FQPSK-JR are 0.14 and 0.17 dB for PAM and PT, respectively. For SOQPSK-TG, the respective losses are 0.08 and 0.22 dB for PAM and PT. Therefore, the PAM-based detectors have a slight performance edge over the PT-based detectors.

B. Serially Concatenated Systems with Iterative Detection

The block diagram of the serially concatenated system is shown in Figure 7. The SISO modules are "max-log" versions of the ones in [17] and [16] (when we take the log of (14), the dependence on N_0 can be dropped). The soft information exchanged between the two SISOs takes the form of log-likelihood ratios and is scaled by the gains K_1 and K_2 to improve performance [1, 20]. The unconnected input in Figure 7 is zero, and the lower input to the SOQPSK SISO is initialized to zero for the first iteration. There are no termination bits added anywhere in the simulations, and the decoder state metrics are initialized to zero for each iteration. We use the same two outer codes that were used in [1] to facilitate the evaluation of the reduced-complexity systems. In both cases the number of iterations is $N_{\text{it}} = 5$.

The first code is the optimal rate-1/2 four-state convolutional code. The generator polynomials of this code are $g_1 = 5$ and $g_2 = 7$, using the octal representation. The interleaver is an S-random interleaver [21], where the interleaver block size is $N = 2048$ and $S = 32$. We select $K_1 = 0.8$ and $K_2 = 0.75$ in all cases

[3]We point out that (17) is specific to the use of the differential encoder and the differential precoder in Figure 1. If non-differential signaling is used, then the distance values in (17) are unchanged but the entire expression is scaled by 1/2.

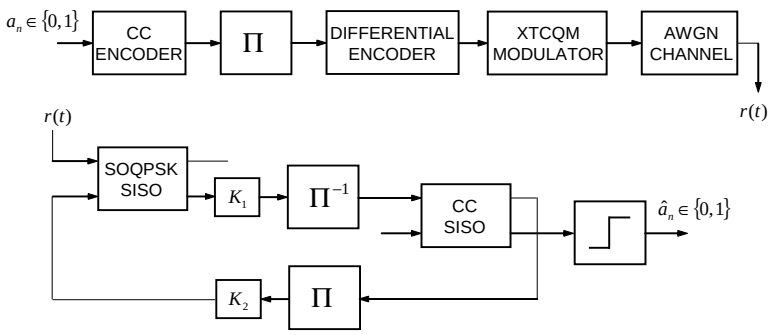

Figure 7: Block diagram of serially concatenated system.

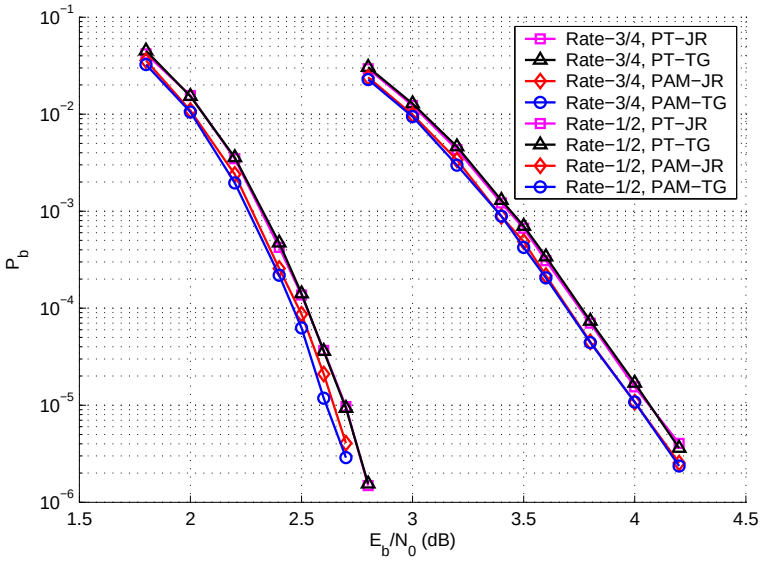

Figure 8: Performance of coded systems.

where the rate-1/2 code is used.

The second code is the optimal rate-3/4 code that is derived from the first code by puncturing two out of every six output bits according to the puncturing matrix [22]

$$\mathcal{P} = \begin{bmatrix} 1 & 0 & 1 \\ 1 & 1 & 0 \end{bmatrix} \tag{19}$$

where zeros represent output bits that are punctured. Here the interleaver properties are $N = 1364$ and $S = 26$. We select $K_1 = 0.7$ and $K_2 = 1$ in all cases where the rate-3/4 code is used.

The performance of these two codes is shown in Figure 8. For SOQPSK-TG, the PAM-based detector has gains of 8.00 dB and 6.60 dB for the rate-1/2 and -3/4 codes, respectively. This is relative to the $P_b = 10^{-5}$ point of the PAM-based detection curve in Figure 6. The PT-based detector has gains of 8.06 and 6.69 dB for the rate-1/2 and -3/4 codes, respectively.

Using the same measurement methodology for FQPSK-JR, the PAM-based detector has gains of 8.14 dB and 6.77 dB for the rate-1/2 and -3/4 codes, respectively. The PT-based detector has gains of 8.11 and

6.75 dB for the rate-1/2 and -3/4 codes, respectively.

As with the uncoded case, the PAM-based detectors have the best overall performance. However, both complexity reduction methods produce large coding gains for these spectrally-efficient modulations, comparable to those reported in [1].

CONCLUSIONS

We have developed reduced-complexity detectors for FQPSK and SOQPSK using a traditional CPM viewpoint. This viewpoint allows the use of well-known approaches for reducing the complexity of partial-response CPM. We explored the use of two such techniques: the PAM approximation and frequency/phase pulse truncation. We have established that the proposed reduced-complexity schemes achieve near-optimal performance with uncoded FQPSK-JR and SOQPSK-TG. We have also shown that the proposed serially concatenated coding schemes achieve large coding gains which are comparable to those recently reported in [1] for MIL-STD SOQPSK.

REFERENCES

[1] L. Li and M. Simon. "Performance of coded OQPSK and MIL-STD SOQPSK with iterative decoding". *IEEE Transactions on Communications*, 52:1890–1900, November 2004.

[2] P.S.K. Leung and K. Feher. "F-QPSK—a superior modulation technique for mobile and personal communications". *IEEE Transactions on Broadcasting*, 39:288–294, June 1993.

[3] Range Commanders Council Telemetry Group, Range Commanders Council, White Sands Missile Range, New Mexico. *IRIG Standard 106-04: Telemetry Standards*, 2004. [Online]. Available: http://jcs.mil/RCC/manuals/106-04.

[4] P. A. Laurent. "Exact and approximate construction of digital phase modulations by superposition of amplitude modulated pulses (AMP)". *IEEE Trans. Commun.*, 34:150–160, February 1986.

[5] E. Perrins and M. Rice. "PAM representation of ternary CPM". submitted to *IEEE Transactions on Communications*, March 2005. See also: E. Perrins and M. Rice, "PAM Representation of Ternary Continuous Phase Modulation", *Department of Electrical and Computer Engineering*, Brigham Young University, February 2005. [Online]. Available: https://dspace.byu.edu/handle/1877/58.

[6] A. Svensson, C-E. Sundberg, and T. Aulin. "A class of reduced-complexity Viterbi detectors for partial response continuous phase modulation". *IEEE Transactions on Communications*, 32:1079–1087, Oct. 1984.

[7] M. Simon and T.-Y Yan. Cross-Correlated Trellis-Coded Quadrature Modulation. U.S. patent filed Oct. 1999.

[8] M. Simon and T.-Y Yan. (1999, May) Performance evaluation and interpretation of unfiltered Feher-patented quadrature phase-shift keying (FQPSK). *Telecommun. and Mission Operations Prog. Rep.*, [Online]. Available: http://tmo.jpl.nasa.gov/tmo/progress_report/42-137/137C.pdf.

[9] M. Simon and T.-Y Yan. "Unfiltering Feher-patented quadrature phase-shift keying (FQPSK): Another interpretation and further enhancements: Parts 1, 2. *Appl. Microwave Wireless Mag.*", 12:76–96/100–105, Feb./Mar. 2000.

[10] R. Jefferis. "Evaluation of constant envelope offset quadrature phase shift keying transmitters with a sofware based signal analyzer". In *Proceedings of the International Telemetering Conference*, October 2004.

[11] S. Benedetto, D. Divsalar, G. Montorsi, and F. Pollara. "Serial concatenation of interleaved codes: Performance analysis, design, and iterative decoding". *IEEE Transactions on Information Theory*, 44:909–926, May 1998.

[12] T. Nelson, E. Perrins, and M. Rice. "Common detectors for shaped offset QPSK (SOQPSK) and Feher-patented QPSK (FQPSK)". To appear in *Proceedings of the IEEE Global Telecommunications Conference (GLOBECOM'05)*, November/December 2005.

[13] J. B. Anderson, T. Aulin, C-E. Sundberg. *Digital Phase Modulation*. Plenum Press, New York, 1986.

[14] B. E. Rimoldi. "A decomposition approach to CPM". *IEEE Transactions on Information Theory*, 34:260–270, March 1988.

[15] D. I. S. Agency. "Department of Defense interface standard, interoperability standard for single-access 5-khz and 25-khz UHF satellite communications channels". Tech. Rep. MIL-STD-188-181B, Department of Defense, March 1999.

[16] S. Benedetto, D. Divsalar, G. Montorsi, and F. Pollara. "A soft-input soft-output AP module for iterative decoding of concatenated codes". *IEEE Communications Letters*, 1:22–24, January 1997.

[17] P. Moqvist and T. Aulin. "Serially concatenated continuous phase modulation with iterative decoding". *IEEE Transactions on Communications*, 49:1901–1915, November 2001.

[18] M. Simon. *Bandwidth-Efficient Digital Modulation With Application to Deep-Space Communication*. Wiley, New York, 2003.

[19] M. Geoghegan. "Optimal linear detection of SOQPSK". In *Proceedings of the International Telemetering Conference*, October 2002.

[20] D. Kim, T. Kwon, J.R. Choi, and J.J. Kong. "A modified two-step SOVA-based turbo decoder with a fixed scaling factor". In *Proceedings of IEEE International Symposium on Circuits and Systems*, October 2000.

[21] D. Divsalar and F. Pollara. (1995, May) Multiple turbo codes for deep-space communications. *Telecommunications and Data Acquisition Progress Report*, [Online]. Available: http://tmo.jpl.nasa.gov/tmo/progress_report/42-121/121T.pdf.

[22] Y. Yasuda, K. Kashiki, and Y. Hirata. "High-rate punctured convolutional codes for soft decision Viterbi decoding". *IEEE Transactions on Communications*, 32:315–319, Mar. 1984.